

A Study of Dense Suspensions Climbing Against Gravity

Xingjian Hou and Joseph D. Peterson

*DAMTP, Centre for Mathematical Sciences, University of Cambridge, CB3 0WA,
United Kingdom*

Abstract

Dense suspensions have previously been shown to produce a range of anomalous and gravity-defying behaviors when subjected to strong vibrations in the direction of gravity. These behaviors have previously been interpreted via analogies to inverted pendulums and ratchets, language that implies an emergent solid-like structure within the fluid. It is therefore tempting to link these flow instabilities to shear jamming (SJ), but this is too restrictive since the instabilities can also be observed in systems that shear thicken but do not shear jam. As an alternative perspective, we re-frame earlier ideas about “ratcheting” as a “negative viscosity” effect, in which the cycle-averaged motion of a vibrated fluid is oriented opposite to the direction implied by the cycle-averaged stresses. Using ideas from the Wyart and Cates modeling framework, we predict that such a “negative viscosity” can be achieved in shear flows driven by oscillating stress with both square and sinusoidal wave forms. We extend this same modeling approach to study falling films in a vibrating gravitational field, where we similarly find it is possible to attain an overall flow opposite the direction of gravity. Preliminary experimental findings are also provided in support of the modeling work.

1 Introduction

A dense suspension comprises solid particles suspended in fluid, with particle density high enough that the rheological properties are dominated by the system’s proximity to a “jamming” transition.

Suspensions of solid particles in a viscous fluid are found in applications ranging from construction to comestibles . The ubiquity of so-called “dense suspensions” can be partly explained by the difficulties encountered in transporting dry powders - dense suspensions do not generate dust, they do not cake, and they are probably less susceptible to flow-induced segregation effects [1]. Besides their relative ease of processing, high density particulate loading can also improve the viscosity/texture of fluid products like paint and toothpaste.

In dense suspensions, there exists a theoretical maximum density at which particles can be packed together without “jamming” the fluid and obstructing flow. Proximity to jamming can be varied simply by changing particle density, but under steady flow one must also consider different modes of jamming and changes in the type of particle-particle contacts present within the system [2, 3]. In particular, high stresses can induce a transition from “sliding contacts” to “frictional contacts” [4, 5, 6], where the latter has fewer degrees of freedom and can therefore produce jammed structures at lower particle densities [7, 8]. The viscosity diverges as constraints are added and degrees of freedom are removed, in some cases culminating with a "jamming" transition in which the fluid becomes rigid in response to continued strain in the same direction [9, 10]. In recent years, there has been growing interest in tuning/controlling the rheological properties of a dense suspension by applying vibrations that manipulate the relative proportion of sliding and frictional contacts [11, 12, 13]. In these studies, vibrations are always introduced as a shear flow orthogonal to the principal flow direction.

Vibrations parallel to flow have received comparatively little attention, except perhaps indirectly in the context of vertically vibrated dense suspensions (VVDS). Studies of VVDS apply vibrations parallel to gravity, often yielding dramatic results that defy ordinary expectations. Early experiments showed that persistent holes can occur at the surface of VVDS [14], as though the fluid contained a ring of elastic material propping the hole open. With increasing acceleration the holes delocalize and more complex structures emerge [14], and subsequent studies have classified a range of gravity-defying structures including rivers, fingers, and jumping liquids [15]. Shinbrot et al [16] have also studied a similar problem, in which dense suspensions showed apparent “climbing” behaviors in the presence of a vertically vibrating probe.

In all the aforementioned phenomena, VVDS were observed to move up/maintain shapes against the influence of gravity. As unusual as these observations may seem, motion against gravity has some precedent in both rigid body mechanics and fluid mechanics, which we summarize briefly here.

In classical mechanics, there is some precedent for vertical vibrations favoring mo-

tion against gravity: most notably, the inverted vibrating pendulum [17] and simple ratcheting mechanisms. Some have attempted to extend this analogy for interpreting the behavior of VVDS [18], but this explanation may be somewhat limited as it fails to account for the fundamentally fluid-like character of the material.

For Newtonian droplets, there is also precedent for vertical vibrations favoring motion against gravity [19], where an interplay between inertial and capillary forces allows isolated droplets to climb up a *partially inclined* surface. However, this climbing mechanism does not apply to behaviors seen in bulk VVDS, nor does it permit climbing on surfaces fully inclined to 90° . We also mention the usual Faraday wave instability, where a quiescent surface develops a standing wave pattern, but does not exhibit any continuous climbing behavior [20, 14].

For ordinary shear thickening fluids, Deegan [21] explained climbing behaviors in terms of discontinuous shear thickening and stress hysteresis in the underlying flow curve. Later simulation work by Shinbrot et al [16] proposed that a “ratcheting mechanism” might occur for fluids climbing up a vertically vibrating probe, using similar arguments as Deegan but with a less mathematically precise framing. However, the simulations by Shinbrot et. al. only required continuous shear thickening, which suggests a separate climbing mechanism independent of stress hysteresis. Comparing the ideas from Deegan et. al. and Shinbrot et. al. we suggest that the source of vibrations (vibrating platform vs vibrating external probe) may play a more important role than one might initially expect.

A range of “climbing” behaviors can also be found in shear flows between concentric cylinders, especially where there are Reynolds stresses (convective acceleration) [22, 23], or elastic stresses (rod climbing) [24, 25] at work. Climbing behaviors such as these are typically explained in terms of normal-stress differences and/or curved streamlines, and are generally well understood. The mechanisms for climbing in VVDS mentioned earlier have so-far excluded any discussion on curved streamlines and normal stress differences, but this may be an interesting subject for future inquiry.

For a general explanation of climbing behaviors in VVDS, the stress hysteresis mechanism proposed by Deegan appears to be most promising, and in this paper we provide follow-up analysis to (1) explicitly connect the hysteresis mechanism to changes in inter-particle contacts and (2) generalize the “ratcheting” idea to a more generic notion of “negative apparent viscosity”. These ideas will be supported by calculations from the Wyart and Cates (WC) modeling framework and new experimental evidence of sustained “climbing” behavior in VVDS.

The organization of our paper is as follows: Section 2 outlines the methods of

our study, including both the governing equations for the Wyart-Cates (WC) theory [8] (section 2.1) and describes the setup of a proof-of-principle experiment (section 2.2). Section 3 presents calculations, using the WC model, for average shear rate under oscillating shear stress (sections 3.1 and 3.2) and average flow rate in a falling film under oscillating gravity (sections 3.3 and 3.4). We also provide a limited discussion on the effect of finite inertia (section 3.5). Section 4 describes the results of our experimental efforts and provides an interpretation of those results following the modeling work of section 3. Section 5 summarizes the results of our study and suggests directions for future research.

2 Methods

In this paper, we aim to demonstrate how the inducement of frictional contact in both discontinuous shear thickening (DST) and shear jamming (SJ) suspensions can help explain observations of gravity-defying flow in vertically-vibrated dense suspensions (VVDS). To achieve this, we require a modeling tool that (1) relates rheology to fluid microstructure, (2) is large in scale compared to particle size (i.e. continuum models), (3) is suitable for reversing flows, (4) is suitable for spatially-resolved flows, and (5) has minimal complexity. It is our view that no existing modelling approach will satisfy all of these demands, and so we defer to WC as a minimal model for preliminary study with acknowledged weaknesses in criterion (3) and (4). These weaknesses are discussed in more detail at the end of section 2.1.

In our experimental efforts, we will aim to conduct proof-of-principle tests for the basic model predictions, and also provide some new experimental results that more unambiguously isolate the “climbing” behavior of VVDS. Future experimental efforts in this vein will require more precise equipment for a systematic study.

The subsections that follow provide a more complete description of the modeling tools and experimental setup that support the results in sections 3 and 4, respectively.

2.1 Theory

To qualitatively capture continuous/discontinuous shear thickening phenomena in dense suspensions, we will leverage modeling tools previously introduced by Wyart and Cates (WC) [8]. To adapt WC to time-dependent flows, we simply exchange the steady shear rate for our time-dependent shear rate.

The physical picture underlying the WC model is summarized as follows: at low

stresses, particles are always separated by a thin lubrication layer that allows for sliding contacts. Above a critical stress, however, lubrication films begin to collapse and particles experience a frictional contact that permits rolling but restricts sliding. With increasing stress, more contacts become frictional and the contact network becomes more constrained in its available movements, leading to shear thickening at the bulk scale. This physical picture is captured mathematically by the WC model equations below:

$$\begin{aligned}\sigma &= \eta \dot{\gamma}, \eta = \frac{\eta_0}{(\phi - \phi_J)^2}, \\ \phi_J &= f \phi_R + (1 - f) \phi_S, \\ f &= \exp\left(-\frac{\sigma^*}{\Pi}\right)\end{aligned}\tag{1}$$

where $\dot{\gamma}$ is the shear rate of the suspension, σ is the shear stress on the suspension, $\Pi = \text{tr}(\mathbf{\Sigma}/3)$ is the particle pressure with $\mathbf{\Sigma}$ being the particle stress tensor (note that σ denotes the xy component of $\mathbf{\Sigma}$ in our work). For steady simple shear flow, the particle pressure $\Pi = \text{tr}(\mathbf{\Sigma}/3)$ should be positive and proportional to the shear stress $\Pi \propto |\sigma|$, and for our purposes the constant of proportionality can be absorbed into the choice of σ^* , which is the critical stress needed to drive particles into contact. For a given fraction of frictional contacts, f , Eq. 1 prescribes a jamming fraction ϕ_J that interpolates linearly between the jamming fraction for purely sliding constraints, ϕ_S , and purely rolling constraints, ϕ_R . Note that f is a function of the scaled particle pressure $|\sigma|/\sigma^*$, with frictional contacts being favored for large particle pressures. For the purpose of this paper, we will assume $\phi_R = 0.57, \phi_S = 0.64$. The viscosity of the suspension η is related to the actual volume fraction of the suspension ϕ . The pre-factor in the Krieger–Dougherty equation [26] is denoted by η_0 and is proportional to the viscosity of the suspending fluid.

The principal success of the WC model is its ability to qualitatively capture a progression from continuous shear thickening (CST) to discontinuous shear thickening (DST) and shear jamming (SJ) with increasing particle volume fraction. In Fig. 1, we plot example “flow curves” for the shear stress σ as a function of the shear rate $\dot{\gamma}$ over a range of volume fractions ϕ covering this transition. Given the assumed values $\phi_R = 0.57, \phi_S = 0.64$, the WC model predicts that hysteresis and DST occur in the range $0.555 < \phi < 0.64$. For $0.57 \leq \phi < 0.64$, it is possible for SJ to occur, i.e. obtaining $\dot{\gamma} = 0$, once σ exceeds a critical value. For $\phi < 0.555$, only CST is observed.

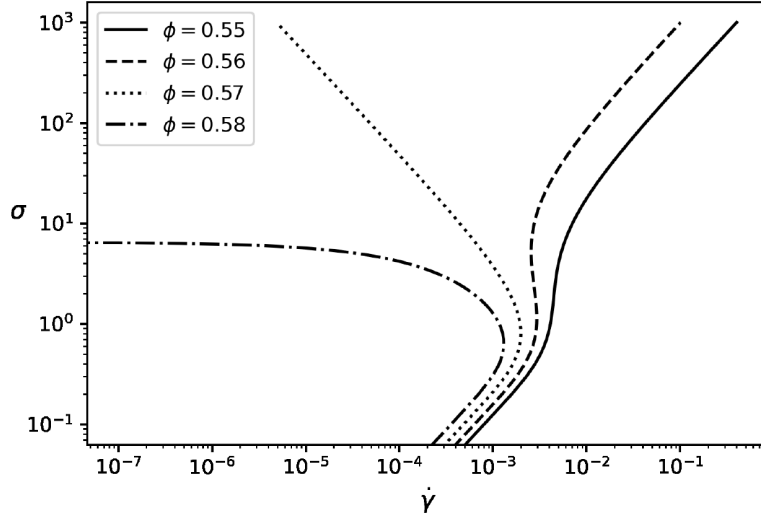


Figure 1: Predictions from the Wyart and Cates (WC) model (Eq. 1) for the steady shear stress σ as a function of shear rate $\dot{\gamma}$ for particle volume fractions $\phi = 0.55, 0.56, 0.57, 0.58$, assuming WC parameters $\phi_R = 0.57, \phi_S = 0.64, \sigma^* = 1, \eta_0 = 1$.

Where the shear stress is known, Eq. 1, can be used to determine the corresponding shear rate:

$$\dot{\gamma} = \begin{cases} \frac{\sigma}{\eta_0} \left[(\phi_R - \phi_S) \exp\left(-\frac{\sigma^*}{|\sigma|}\right) + (\phi_S - \phi) \right]^2, & \phi < \phi_J \\ 0, & \phi > \phi_J \end{cases} \quad (2)$$

Eq. 2 can also be generalized for a known time-dependent shear stress, $\sigma(t) = \sigma_0 + \Delta\sigma(t)$. For a forcing that's periodic on time T , we can define an average shear rate $\bar{\dot{\gamma}}$ by:

$$\bar{\dot{\gamma}} = \frac{1}{T} \int_0^T dt \dot{\gamma}(t) \quad (3)$$

Likewise, we can define a cycle-averaged viscosity $\bar{\eta} = \sigma_0/\bar{\dot{\gamma}}$, assuming $\Delta\sigma(t)$ has zero mean. For Newtonian fluids - and indeed for most non-Newtonian fluids, the sign of $\bar{\eta}$ is always positive. However, our calculations in sections 3.1 and 3.2 suggest that this may not always be the case for dense suspensions.

The coupling between fluid motion¹ and fluid stresses in a fluid film is determined by via the Navier-Stokes equation, conserving momentum:

¹For convenience, equation 4 is written in the frame of the vibrating support. In the lab frame the suspension is under constant gravity \mathbf{g}_0 and the support vibrates parallel to gravity with acceleration $-\Delta\mathbf{g}(t)$ of period T , so the equivalent gravity is $\mathbf{g}(t) = \mathbf{g}_0 + \Delta\mathbf{g}(t)$ in the vibrating frame.

$$\rho\left(\frac{\partial \mathbf{u}}{\partial t} + \mathbf{u} \cdot \nabla \mathbf{u}\right) = -\nabla p + \nabla \cdot \boldsymbol{\sigma} + \rho \mathbf{g} \quad (4)$$

We also assume an incompressible flow:

$$\nabla \cdot \mathbf{u} = 0 \quad (5)$$

For uni-direction flow, $\mathbf{u} = u_x \mathbf{e}_x$, and Eq. (3) becomes:

$$\rho \frac{\partial u}{\partial t} = \frac{\partial \sigma}{\partial x} + \rho g_x \quad (6)$$

Eq. 6 will be applied to model oscillatory shear flows, $g_x = 0$, and falling films under oscillating gravity, $g_x = g_0 + \Delta g(t)$, where g_0 is normal gravity and $\Delta g(t)$ is a zero-mean oscillation.

For the remainder of this report, we will conduct our analysis in terms of non-dimensionalized equations. A set of characteristic scales is defined to non-dimensionalize Eq. 6. The time scale is $\tau_C = T$, the period of oscillation. The length scale is $y_c = H$, the thickness of the fluid film. We assign a stress scale σ_C on the basis of the average forcing: for flows driven by an oscillating shear stress $\sigma(t)$ of period T , we choose $\sigma_C = \sigma_0$, where $\sigma_0 = \frac{1}{T} \int_0^T dt \sigma(t)$ is the average shear stress. For falling film flow driven by oscillating gravity $g_x(t)$, we choose $\sigma_C = \sigma_0$ where $\sigma_0 = \rho g_0 H$ gives the wall shear stress for a Newtonian fluid under fixed gravity $g_0 = \frac{1}{T} \int_0^T dt g_x(t)$. Given these characteristic stresses, we use the zero shear viscosity of the fluid $\eta_{\dot{\gamma}=0}$ to estimate a characteristic velocity, $u_C = H \sigma_C / \eta_{\dot{\gamma}=0}$. Rescaling all variables in this way, we obtain:

$$\text{Re} \frac{\partial}{\partial t} u = -\frac{g_x}{g_0} + \frac{\partial \sigma}{\partial x} \quad (7)$$

where:

$$\text{Re} = \left(\frac{H^2 \rho}{\eta_{\dot{\gamma}=0} T} \right) \quad (8)$$

The Reynolds number is a dimensionless variable comparing the typical scale of inertial forces to viscous forces. For the purpose of study, we assume $\text{Re} \ll 1$, as we are interested in high viscosity fluids, $\eta_{\dot{\gamma}=0} \sim 1 \text{Pa}\cdot\text{s}$, small lengthscales, $H \sim 1 \text{mm}$, and modest cycle times, $T \sim 0.1 \text{s}$. The system is also influenced by (1) the typical stresses in the fluid relative to the stress required for frictional contact σ_0 / σ^* , where $\sigma_0 = \sigma_C$ for a fluid film; (2) the relative amplitude of the oscillations $\Delta \sigma / \sigma_0$, $\Delta g / g_0$, where $\Delta \sigma$, Δg is the amplitude of the oscillations $\Delta \sigma(t)$ and $\Delta g(t)$.

In the introduction to this section, we noted that there are at least two major limitations to this modeling approach. To close this section, we expand upon those limitations in more detail.

First, WC is strictly suited to steady shear flows and cannot account for time-dependent flows, reversing flows, and it lacks a tensorial structure for general 3D flows [27, 13, 8]. Unfortunately, existing models that overcome these limitations have considerably higher complexity [13] and are still limited in many respects (see next paragraph). In any case, we feel that a minimal model like WC is appropriate for a preliminary study, provided one keeps the model’s limitations in mind through the final analysis.

Second, WC is not suited for spatially resolved flows in which one can encounter particle migration [28, 29] and non-local microstructure relaxation processes [30], neither of which are included in our present approach. These physics may be of particular relevance where there is an unstable section of a dense suspension’s flow curve [31, 32, 33, 34], and this is the portion of the flow curve most relevant to our proposed mechanism for a “negative viscosity” effect. However, to our knowledge there is not yet an established modeling framework that would address all of these concerns, and so we once again defer to the simpler WC model.

With respect to both of the limitations above, we are effectively assuming that the WC model captures essential features of flows with DST even where it fails to capture the details of how those flows develop spatially and temporally. This is a severe approximation, but it is also a reasonable concession given the limitations in the current space of available modeling tools.

2.2 Experiments

In the experiment, an oscillating signal is generated via an online tone generator [35] connected to a digital amplifier (Lepy Lp 2020A). A loudspeaker (Pyle PLMR61B, 120W) connects to the amplifier, providing oscillation. To contain the fluid, we adhered a plastic container (dimensions 10cm diameter, 4cm height) to the surface of the loudspeaker using hot-melt adhesive. Experiments were conducted with the plastic container alone or with additional structures attached, including (as seen in Fig. 2) a plastic straw (1.2 cm diameter, 20 cm height).

In the experiment, the frequencies of oscillations range between $1 \sim 25Hz$. At 10Hz, where many of our experiments were conducted, the maximum peak-to-peak displacement was observed to be approximately 1cm, corresponding to a peak acceleration of

$$\Delta g \approx 20m/s^2.$$



Figure 2: Experimental setup: The loudspeaker and the digital amplifier connected to each other. A plastic container was adhered to the loudspeaker to contain the fluid. Experiments were conducted with the plastic container alone or with additional structures attached, including a plastic straw.

3 Modeling Results

In this section we will employ Eqs. 1 and 7 (with $Re = 0$) to model the effect of vibrations/oscillations parallel to the direction of flow, especially as it pertains to a cycle-averaged shear rate $\bar{\dot{\gamma}}$ (oscillating shear flows, sections 3.1 and 3.2) or a cycle-averaged flow rate (oscillating falling films, sections 3.3 and 3.4). Finally, in section 3.5, the effect of finite inertia on the motion of fluid film with sinusoidal forcing is discussed and it is found that a small amount of inertia gives a first correction term that averages to zero.

Before proceeding with detailed calculations, we first provide a general discussion on the underlying mechanism by which one might obtain an apparent negative viscosity from a dense suspension. Fig. 3(a) gives the flow curve for a sample CST fluid, $\phi = 0.55 < 0.555$. Here, shear rates always increase with increasing shear stress, and it is not possible to choose a set of points along the flow curve for which the average shear rate and the average shear stress do not have the same sign. However, for a DST fluid like that shown in Fig. 3(b), there is a portion of the flow curve where the shear stress is decreasing with increasing shear rate. Neglecting, for the moment, concerns over the stability of these portions of the flow curve, it is now possible to choose a pair of points (e.g. corresponding to the start of the high viscosity branch at positive shear rates and

the end of the low viscosity branch at negative shear rates) such that the average shear rate $\bar{\dot{\gamma}} = (\dot{\gamma}_1 + \dot{\gamma}_2)/2$ corresponds to motion opposite direction to average shear stress $\sigma_0 = (\sigma_1 + \sigma_2)/2$, thus giving the appearance of a “negative viscosity”.

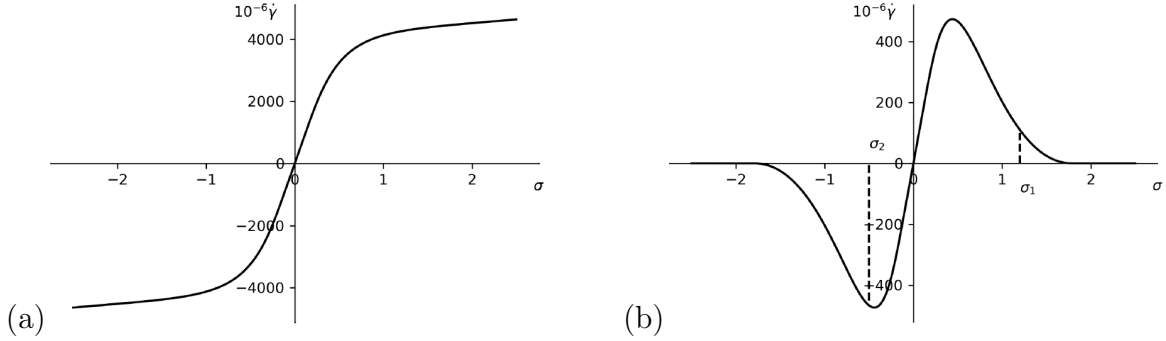


Figure 3: (a) Shear rate $\dot{\gamma}$ - stress σ relationship for suspension with $\phi = 0.55$. It is impossible to obtain σ_1, σ_2 such that $\sigma_1 + \sigma_2 > 0, \dot{\gamma}_1 + \dot{\gamma}_2 < 0$. (b) Shear rate $\dot{\gamma}$ - stress σ relationship for suspension with $\phi = 0.6$. It is possible to obtain σ_1, σ_2 such that $\sigma_1 + \sigma_2 > 0, \dot{\gamma}_1 + \dot{\gamma}_2 < 0$.

This proposed mechanism makes no special distinction between SJ and DST materials - the “negative viscosity” effect is made possible through the existence of a turning point in the underlying flow curve. How and where a “negative viscosity” effect appears may vary depending on the details of the underlying flow curve and the time-dependent stress protocol, as we will see in the sections that follow.

Here, we again remind the reader that our modeling approach carries two limitations with respect to the above proposed mechanism as discussed in section 2.1: namely, the WC model is not really equipped to model unsteady or spatially resolved flows, as is necessary for any proper study of the unstable branch of the flow curve [31, 28, 33, 32, 34]. In light of these limitations, we have argued that the use of WC is justified if one expects that the basic hysteretic structure of the WC flow curve is more or less preserved even where a uniform flow is not attainable.

To partially assuage concerns over the simplicity of our modeling approach, we assure the reader that 2D particle-based simulations using the critical load model [6] affirm the premise of our mechanism for a “negative viscosity” effect. The results shown in Figure 4 were generously contributed by by Roman Mari. These proof-of-principle calculations consider a bi-disperse collection of 100 discs (66 of size 1, 34 of size 1.4) with a friction coefficient of 2, covering an area fraction of 0.78. The forward and reverse shear are produced via a square-wave shear stress protocol, alternating 50 units of time at +20

critical stress units followed by 50 units of time at $-1/20$ critical stress units. Under large positive stress, the system jams and ceases to flow such that the small negative stress dominates the cycle-averaged shear rate, as evidenced by the negatively-sloping trend line in accrued strain over time.

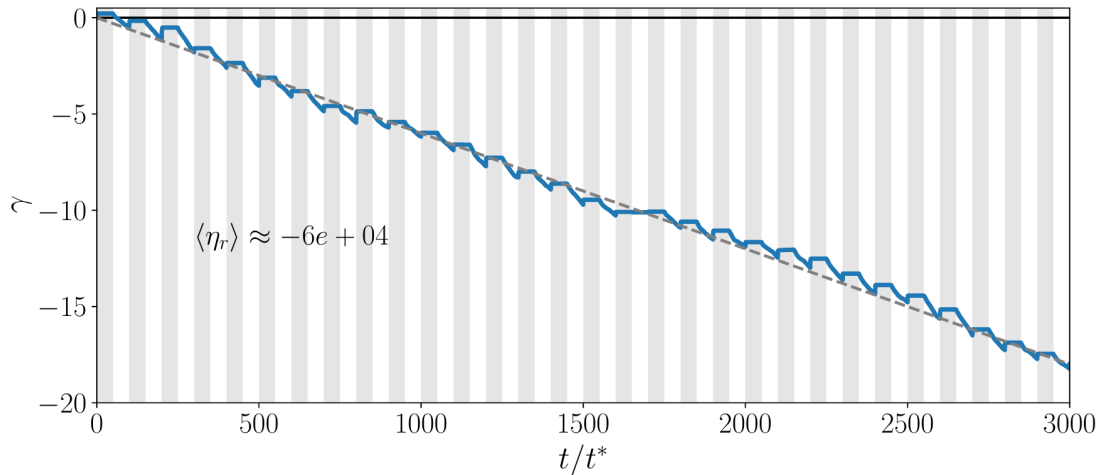


Figure 4: Accrued strain as a function of time for particle-based calculations of the 2D critical load model. The calculations considered a bi-disperse collection of 100 discs (66 of size 1, 34 of size 1.4) with a friction coefficient of 2, covering an area fraction of 0.78. The forward and reverse shear are produced via a square-wave shear stress protocol, alternating 50 units of time at $+20$ critical stress units followed by 50 units of time at $-1/20$ critical stress units. The negative sloping trend line indicates that strain is occurring opposite to the average stress, and the slope of the curve provides an estimate of the apparent viscosity.

Thus, while we acknowledge that our choice of constitutive model is limiting, we are confident that the underlying premise of our proposed mechanism is basically sound. Follow-up studies seeking a quantitative confrontation to experimental results or particle-based simulations will benefit from more detailed constitutive modeling tools, but for the time being it is our view that the WC model provides the best balance of microscopic insight and computational simplicity.

As a closing note to this introductory section, our use of the term “negative viscosity” should be understood as an interpretative framework rather than an actual material property. A simple way to demonstrate the limitations of this interpretive framework is to consider the possibility of a “zero viscosity” effect, where the time-averaged stress is zero but the time-averaged shear rate is non-zero. Our study only looks at time-

symmetric oscillations, where a zero-average stress is only possible for a zero-average shear rate, but for time-asymmetric oscillations a “zero viscosity” may indeed be possible. However, in such cases the directionality of the flow is predetermined by the asymmetry of the forcing (and unchanged by small perturbations to the stress) so it is not clear that a “zero viscosity” effect would exhibit any non-trivial behaviors beyond those already discussed for a “negative viscosity” effect.

3.1 Square-wave Oscillations in Shear Stress

In this section, we will consider flow driven by a defined time-dependent shear stress following a square-wave variation in time:

$$\sigma(t) = \begin{cases} \sigma_0 + \Delta\sigma & \text{if } t \pmod{1} < 1/2 \\ \sigma_0 - \Delta\sigma & \text{if } t \pmod{1} \geq 1/2 \end{cases} \quad (9)$$

From Eq. 9, we see that shear stress alternates between $\sigma_1 = \sigma_0 + \Delta\sigma$ and $\sigma_2 = \sigma_0 - \Delta\sigma$ over equal time periods. The shear rate evolution over a period is shown in Fig. 5(a).

Fig. 5(b) shows average shear rates $\bar{\gamma}$ under different $\sigma_0, \Delta\sigma$. Negative shear rates can only be achieved for $\Delta\sigma/\sigma_0 > 1$ as this is the minimum condition for any negative stress to appear at all. For higher $\Delta\sigma/\sigma_0$ and σ_0/σ^* however, there can be zero shear rate where the system is jammed.

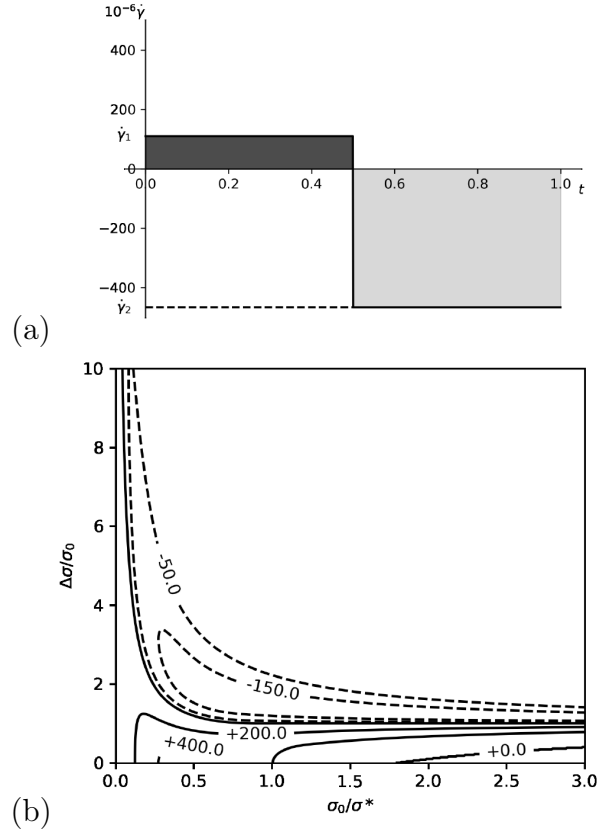


Figure 5: (a) Strain rate $\dot{\gamma}$ evolution of $\phi = 0.6$ over a period of square-wave stress with $\sigma_0/\sigma^* = 0.35, \Delta\sigma/\sigma_0 = 2.4$. (b) Average shear rates $10^{-6}\bar{\gamma}$ of suspension of volume fraction $\phi = 0.6$ under square wave stresses of different average stresses σ_0/σ^* and oscillation amplitudes $\Delta\sigma/\sigma_0$.

As shown in Fig. 6, negative shear rates cannot occur for $\phi = 0.55 < 0.555$ without DST, while they can occur for $0.555 < \phi < 0.64$ with DST or SJ. One key distinction between the DST, and SJ regime is that for DST materials the band of conditions where negative shear rates are seen is bounded by regions where the average shear rate is always positive (c.f. Fig. 6(b)), where SJ fluids lack the second space of positive shear rates (c.f. Fig. 6(c)-(d)). For DST fluids the transition back to positive shear rates corresponds to scenarios where positive shear rates along the high friction branch dominate, and this branch of the flow curve does not exist where shear jamming takes place.

In Fig. 6(c), we see the transition from DST to SJ, for which the combination of large stresses and large oscillations always produces a negative shear rate with absolute value tending towards zero. Simply put, when the stresses become large, the fluid will

be very nearly jammed under both positive and negative stresses, but on balance it will still be more flowable for negative stresses.

For SJ systems $0.57 < \phi < 0.64$ (c.f. Fig. 6(d)) sufficiently large stresses are capable of inducing jamming, i.e. the total cessation of flow $\bar{\gamma} = 0$. The bounding contour for total jamming, $\bar{\gamma} = 0$, is not shown.

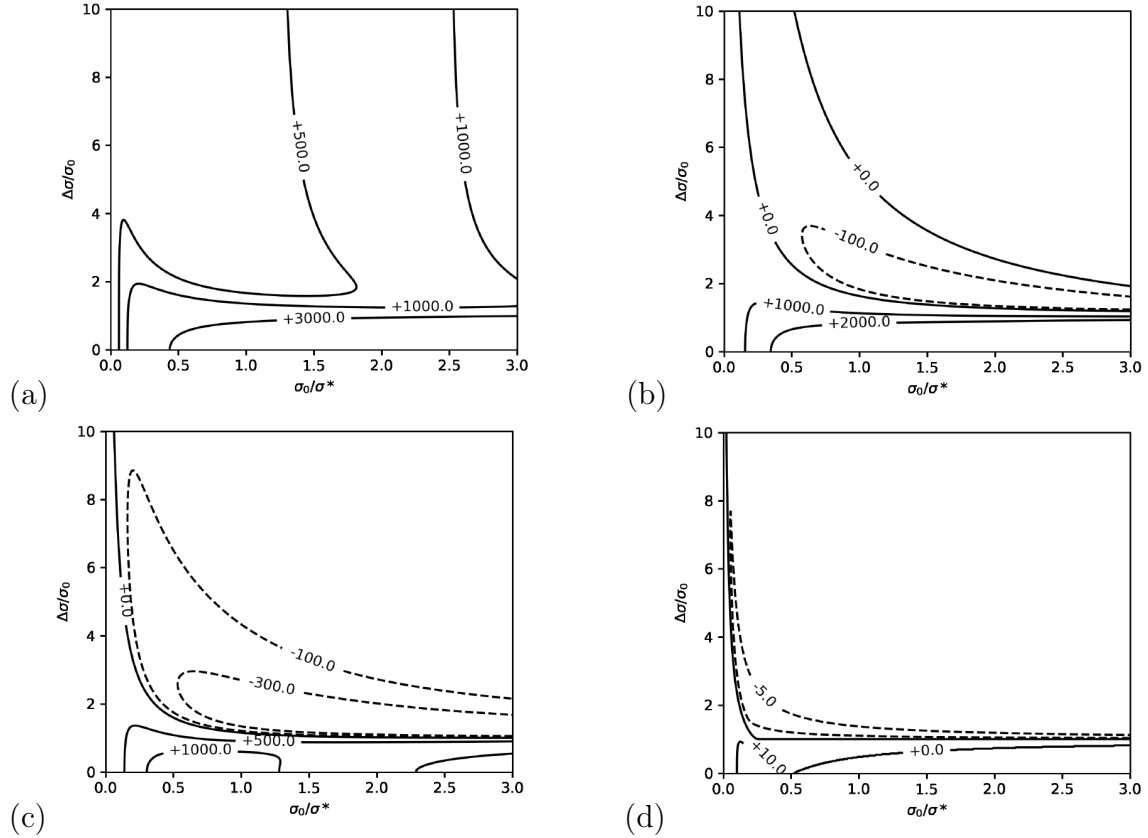


Figure 6: Average shear rates $10^{-6}\bar{\gamma}$ of suspensions of volume fractions ϕ : (a) 0.55 (b) 0.56 (c) 0.58 (d) 0.63 under square wave stresses of different average stresses σ_0/σ^* and oscillation amplitudes $\Delta\sigma/\sigma_0$.

3.2 Sine-wave Oscillations in Shear Stress

Square wave stress protocols are useful for introducing the idea of shear rates opposite to shear stresses in DST fluids, and here we show that the same mechanism extends (albiet less efficiently) to a flow driven by a sinusoidal stress protocol, $\sigma(t) = \sigma_0 + \Delta\sigma\sin(2\pi t)$. The stresses and shear rates at each moment are determined and the shear rates are averaged with Eq. 3.

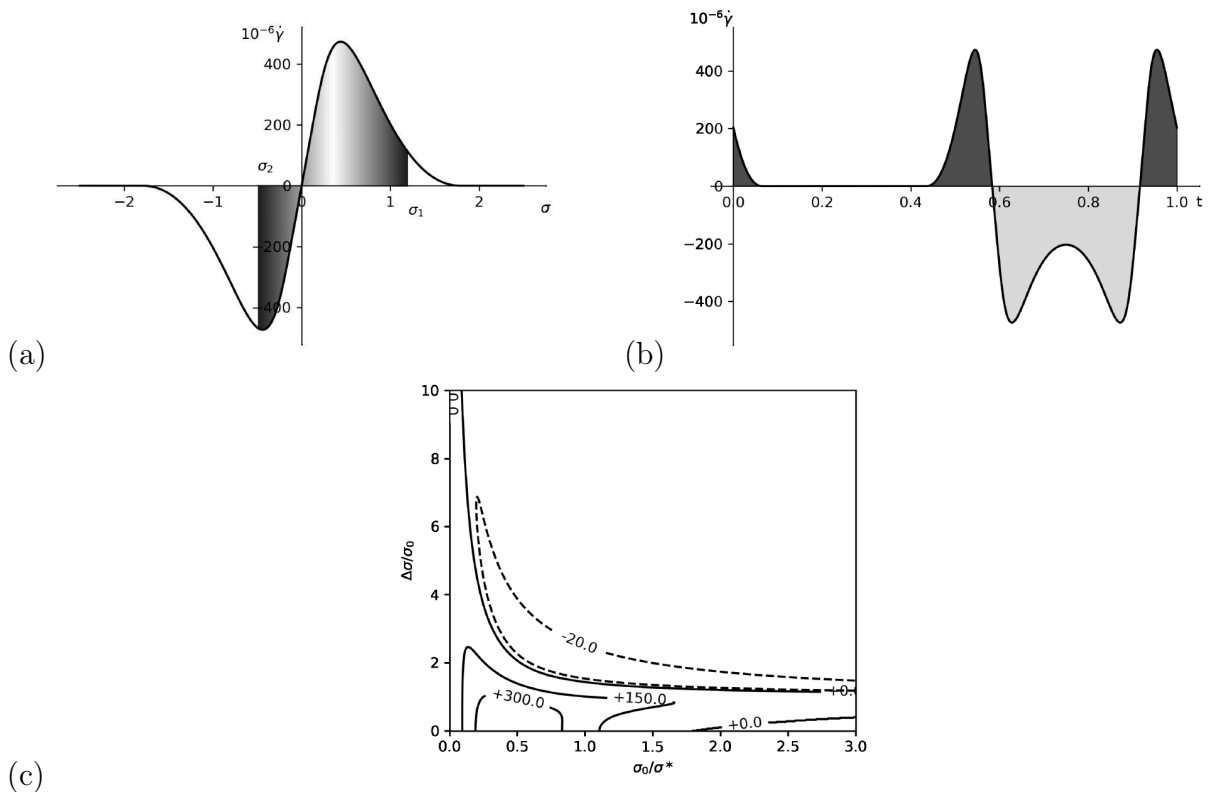


Figure 7: (a) The strain rate $\dot{\gamma}$ - stress σ relationship for suspension with $\phi = 0.6$. The colour gradient demonstrates how much different stresses are weighted when averaging strain rates over a period. (b) The strain rate $\dot{\gamma}$ evolution over a period of sinusoidal stress with average stress $\sigma_0/\sigma^* = 1$, relative amplitude $\Delta\sigma/\sigma_0 = 2$. (c) Average shear rates $10^{-6}\bar{\dot{\gamma}}$ of suspension of volume fraction $\phi = 0.6$ under sinusoidal stresses of different average stresses σ_0/σ^* and relative amplitude $\Delta\sigma/\sigma_0$.

As shown in Fig. 7, the sine wave stress protocol gives predictions similar to those observed in Fig. 5. Here, however, it is harder for negative average shear rates to occur because the fluid spends more time exploring the non-inverted portions of the flow curve with high positive shear rates.

As shown in Fig. 8, negative shear rates can only be observed for $\phi > 0.57$ when the stress protocol is sinusoidal. This is a stricter requirement than the square wave, which only requires DST or $\phi > 0.555$. At high ϕ , the inverted portion of the flow curve is more extended, so large positive shear rates will be explored less by the fluid and it is easier to achieve negative average shear rates.

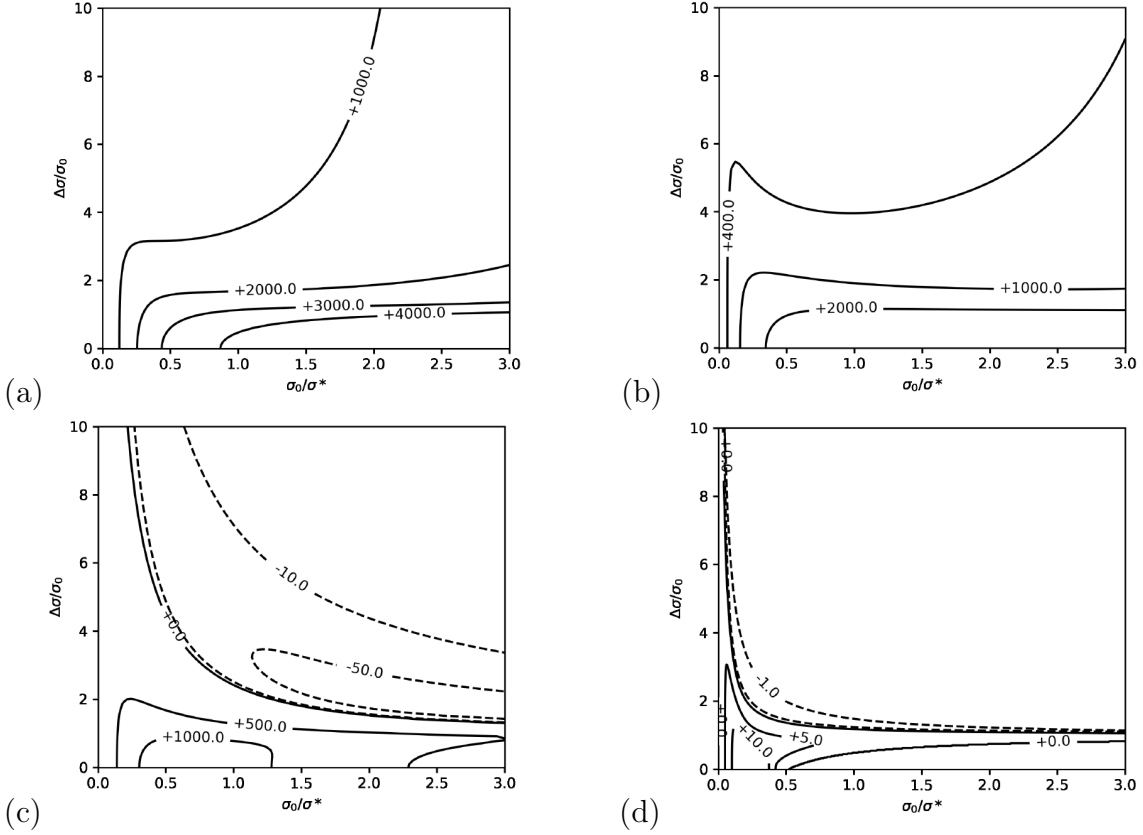


Figure 8: Average shear rates $\dot{\gamma}$ of suspensions of volume fractions ϕ : (a) 0.55 (b) 0.56 (c) 0.58 (d) 0.63 under sinusoidal stresses of different average stresses σ_0/σ^* and relative amplitudes $\Delta\sigma/\sigma_0$.

3.3 Square-wave Oscillations in Gravity

Simple shear flows driven by defined stresses are perhaps the most well-defined means of testing the premise of a “negative viscosity” in vibrated dense suspensions. In this subsection (and the one that follows) we turn our attention to predictions for falling films in oscillatory gravity. The basic premise is still the same: the strength of gravity controls the scale of stresses within the fluid, and there are conditions where the fluid moves faster under weak (reversed) gravity than strong (normal) gravity.

In parallel to our analysis in section 3.1, we first consider the motion of the fluid film under a gravity following a square-wave variation in time:

$$g_x(t) = \begin{cases} g_0 + \Delta g & \text{if } t \pmod{1} < 1/2 \\ g_0 - \Delta g & \text{if } t \pmod{1} \geq 1/2 \end{cases} \quad (10)$$

The motion of the fluid film is described by Eq. 7. We first assume $\text{Re} \sim 0$, so:

$$1 \pm \frac{\Delta g}{g_0} = \frac{\partial \sigma}{\partial x} \quad (11)$$

Taking the free surface as $x = 0$, we have:

$$\sigma = \left(1 \pm \frac{\Delta g}{g_0}\right)x \quad (12)$$

which gives the shear stress at every position of the film $x \in [0, 1]$. The shear rates at each x position are determined from the corresponding shear stresses. The velocity is obtained through integrating shear rates:

$$v(x) = \int_0^x dx' \dot{\gamma}(t, x) + u(t) \quad (13)$$

where $u(t)$ is the velocity of the solid boundary, and over a period $\bar{u}(t) = 0$. Averaging $v(x)$ over each position $x \in [0, 1]$, we can obtain the velocity of the film:

$$\bar{u} = \int_0^1 dx u(t, x) \quad (14)$$

The average velocity over a period is obtained through Eq. 3. Similar to section 3.3, negative values can be obtained for $\Delta g/g_0 > 1$, which is the minimum condition for any stress to appear at all. However, Eq. 12 shows that part of the fluid is constantly under low stress, i.e., in the uninverted portions of the flow curve. This makes it harder to achieve negative \bar{u} as the positive shear rates are explored more by the fluid film.

3.4 Sine-wave oscillations in Gravity

In parallel with the results given in section 3.2, we now extend our analysis to fluid films with gravitational forcing varying sinusoidally in time, $g(t) = g_0 + \Delta g \sin(2\pi t)$. In the case of sine waves, Eqs. 11 and 12 are substituted with

$$1 \pm \frac{\Delta g}{g_0} \cos(t) = \frac{\partial \sigma}{\partial x}, \sigma = \left[1 \pm \frac{\Delta g}{g_0} \cos(t)\right]x \quad (15)$$

The average velocity of the fluid film follows similar calculation procedure as in Eqs. 13 and 14. It is harder to achieve negative velocity than in both sections 3.2 and 3.3, as (1) similar to section 3.3, part of the film is constantly under low stress and (2) the gravity can fluctuate to lower values during oscillation, so the fluid will explore more the positive shear rates.

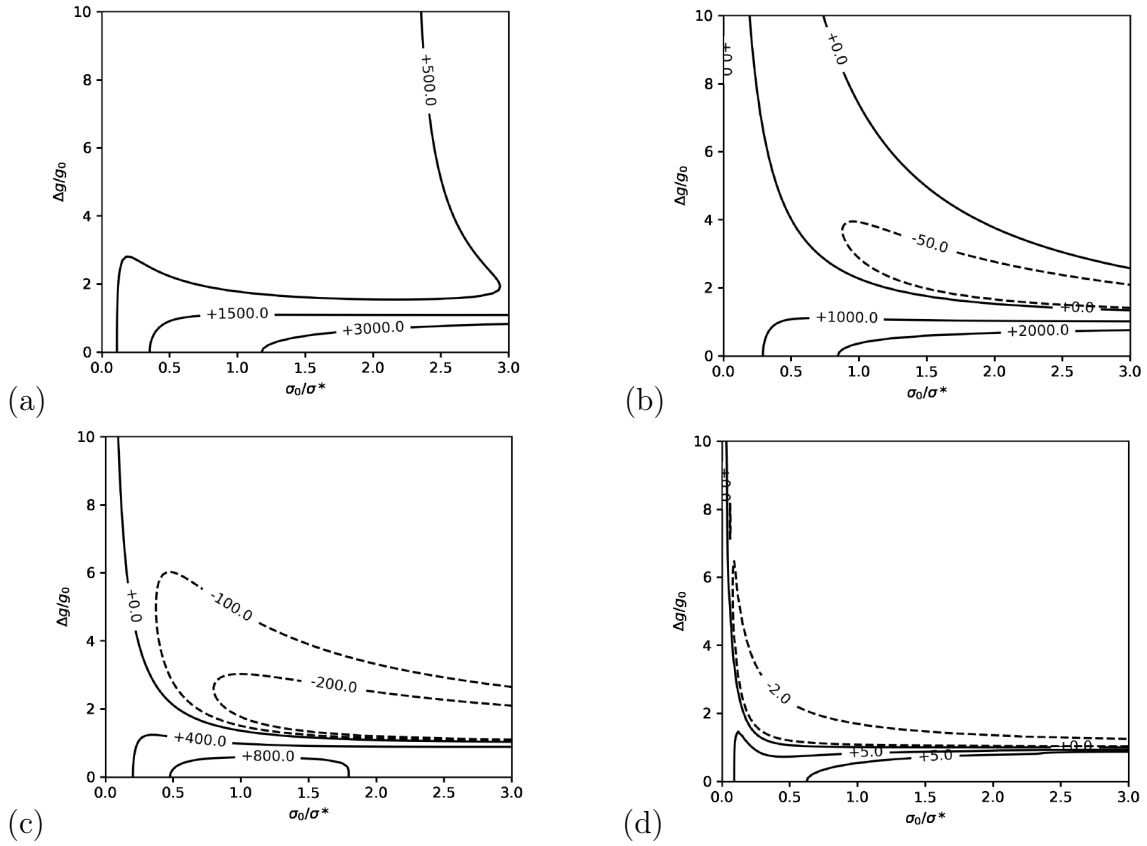


Figure 9: The velocities $10^{-6}\bar{u}$ of falling films of volume fractions ϕ : (a) 0.55 (b) 0.56 (c) 0.58 (d) 0.63 under square-wave gravity of different average stresses σ_0/σ^* (where $\sigma_0 = \rho g_0 H$) and relative amplitudes $\Delta g/g_0$.

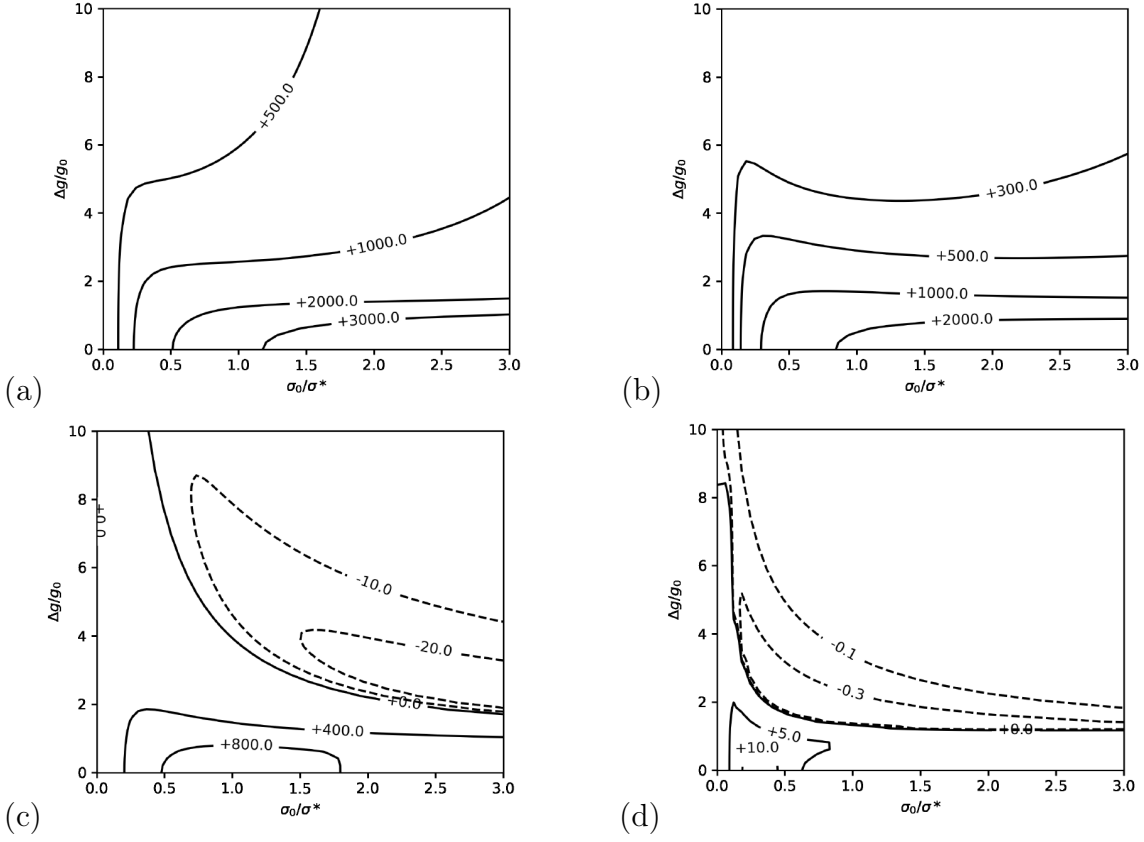


Figure 10: Velocities $10^{-6}\bar{u}$ of films of volume fractions ϕ : (a) 0.55 (b) 0.56 (c) 0.58 (d) 0.63 under sine-wave gravity of different average stresses σ_0/σ^* (where $\sigma_0 = \rho g_0 H$) and relative amplitudes $\Delta g/g_0$.

3.5 Some results for finite inertia

From Eqs. 7 and 8, the finite Reynolds number can be of influence to the fluid motion. In the experiments, $\eta_{\dot{\gamma}=0} \sim 1 Pa \cdot s, H \sim 1 mm, T \sim 0.1 s, \rho \sim 1000 kg/m^3$, so $Re \sim 0.01$. Here we consider an expansion for small Reynolds numbers, $Re \ll 1$, with sinusoidal variations in the gravitational field, as in section 3.4. Our analysis will not extend to consider the stability of a base-state limit cycle to perturbations, where negative-sloping portions of the flow curve have previously been shown to be unstable in steady shear [36].

Eq. (5) is now written as:

$$Re \frac{\partial}{\partial t} u = -\left(1 + \frac{\Delta g}{g_0} \cos(2\pi t)\right) + \frac{\partial \sigma}{\partial x} \quad (16)$$

Expanding $u(t), \sigma(t)$ with respect to Re :

$$\begin{aligned} u(\text{Re}, t) &= u_0(t) + u_1(t)\text{Re} + \dots, \\ \sigma(\text{Re}, t) &= \sigma_0(t) + \sigma_1(t)\text{Re} + \dots \end{aligned} \quad (17)$$

Plugging (13) into (12) we find:

$$0 = \left\{ - \left[1 + \frac{\Delta g}{g_0} \cos(2\pi t) \right] + \frac{\partial \sigma_0}{\partial x} \right\} \text{Re}^0 + \left\{ - \frac{\partial u_0}{\partial t} + \frac{\partial \sigma_1}{\partial x} \right\} \text{Re}^1 + \dots \quad (18)$$

The coefficients for each order of Re should be zero, so:

$$\frac{\partial \sigma_0}{\partial x} = 1 + \frac{\Delta g}{g_0} \cos(2\pi t), \quad (19)$$

$$\frac{\partial \sigma_1}{\partial x} = \frac{\partial u_0}{\partial t} \quad (20)$$

Eq. (15) is an even function about time $t = 1/4$, the same for the velocity $u_0(x, t)$ at any point x under low Re . This also means that $\partial_t u_0(x, t)$ is an odd function about time $t = 1/4$ for any x . So it must also be true that $\sigma_1(x, t) = \int_0^x da \partial_t u_0(a, t)$ is an odd function about $t = 1/4$, since it is just a sum of odd functions.

We also expand $\dot{\gamma}(t)$ with $\dot{\gamma}(\text{Re}, t) = \dot{\gamma}_0(t) + \text{Re}\dot{\gamma}_1(t) + \dots$. For low Re we have:

$$\dot{\gamma}_1 = \frac{\partial \dot{\gamma}}{\partial \sigma}(\sigma_0(x, t))\sigma_1 \quad (21)$$

Where the input to a function is even, then output must also be even, so $\frac{\partial \dot{\gamma}}{\partial \sigma}(\sigma_0(t, y))$ is an even function about time $t = 1/4$.

If we compute the average shear rate on a time $t \in [-1/4, 3/4]$, such that the averaging interval is centered about $t = 1/4$, we are taking the inner product of the odd $\sigma_1(x, t)$ function and the even $\frac{\partial \dot{\gamma}}{\partial \sigma}(\sigma_0(t, y))$ function on the domain, so the integral evaluates to zero.

Thus, to a first correction, a small amount of inertia gives the first correction term $\overline{\dot{\gamma}_1(t)} = 0$. Neglecting considerations of flow stability, the effect of inertia should only appear in an $O(\text{Re}^2)$ correction, with $\text{Re} \approx 0.01$ in this case.

4 Experimental Results

In this section, we will first summarize what we observed in our experimental study (section 4.1) and then follow-up with a discussion of those findings in relation to our

experimental observations (section 4.2).

4.1 Summary of Experimental Observations

The experimental setup has been explained in section 2.2. We used suspensions of cornstarch in water with varying particle mass fractions between 52-55%. To simulate the oscillating gravitational field Δg , we modulate the frequency f and amplitude A of the oscillating speaker platform, $\Delta g = (2\pi f)^2 A$, and $g_0 = 9.8\text{m/s}^2$ is maintained as the constant value of gravity. Our experiments allowed us to access frequencies as low as $f = 1\text{Hz}$ and peak amplitudes as large as about $A = 0.5\text{cm}$, but the simple experimental setup did not permit direct control over the oscillation amplitude A , and the power limitations of our speaker/amplifier setup meant that for frequencies above about 20Hz the maximum displacement amplitude decreased with increasing frequency. In the discussion that follows, adjustments to the amplitude will be described qualitatively in terms of speaker volume settings, in keeping with the level of direct control we had over the experiments themselves.

Between $1 \sim 14$ Hz, the suspension develops Faraday waves when the volume controls were set sufficiently high. For low frequency $1 \sim 10$ Hz, Faraday waves are stable and the suspension does not climb or form stable holes after being finitely perturbed. For frequencies in the range of $12 \sim 14$ Hz, Faraday waves are unstable to finite-amplitude perturbations, and the suspension can continuously climb up after being perturbed.

Between $12 \sim 19$ Hz, columns of the suspension with thickness $\sim 1\text{mm}$ and width $\sim 3\text{mm}$ can climb up vertical surfaces. At frequencies greater than 20 Hz, however, such climbing motion is slowed down, possibly because our experimental setup lacks the power to maintain large accelerations at high frequencies.

At 53% mass fraction of cornstarch, droplets of thickness $1 \sim 2$ mm were observed to climb up at 2mm/s under a sinusoidal signal of 15Hz, 100% volume, with an approximate $\Delta g \approx 89\text{m/s}^2$, corresponding to $\Delta g/g_0 = 8.9$. Droplets were formed on vertical surfaces either without direct intervention (e.g. “pinched off” from climbing columns or splashing up from the reservoir below) or by direct placement, collecting a small amount of fluid and allowing it to wet the surface.

Holes and finger-like structures can appear in the range of $f = 14 \sim 25$ Hz, as previously documented in earlier literature [15]. Within the lower end of this frequency range, $f = 14 \sim 19$ Hz, the delocalized holes and finger-like structures form quickly, rising and falling periodically. At higher frequencies $20 \sim 25$ Hz, the climbing activity

of finger-like structures are quieted, allowing persistent holes to become the dominant stable structure. This transition from fingers to holes with increasing frequency may be an artifact of dampened oscillation amplitude at high frequencies, reflecting a limitation in our experimental setup.

While most of the observed phenomena have been discussed in literature (e.g. faraday waves, holes, and fingers [14][15]), climbing droplets have not been observed previously and are broadly consistent with both the stress hysteresis mechanism suggested by Deegan [21] and our generalization of the same to the notion of a “negative viscosity” effect.

4.2 Discussion and Relationship to Model Predictions

To discuss our experimental findings in relation to the modeling work of section 3, we will need to estimate model parameters and review some assumptions and approximations. Given the lack of precision in our experimental design and the weaknesses of our modeling approach, we feel that it is only appropriate to frame this discussion in qualitative terms and any appearance of quantitative agreement should be understood as fortuitous and insufficient to validate our modeling approach.

First, we will assume that the flow within a rising or falling column of fluid can be idealized in terms of a 1D flow in a falling film, as per sections 3.3 and 3.4. Since the displacement field is varying in a sinusoidal pattern, we will compare against the predictions of Figure 10, requiring estimates of the dimensionless groups $\Delta g/g_0$ and σ_0/σ^* . Because climbing is only apparent in subfigures (c) and (d), these will be the focus of our discussion, though we make no claims as to whether our experiments corresponded to DST or SJ conditions.

To review, the dimensionless group σ_0/σ^* compares the wall stress to the stress for frictional contact in the case of a vertical falling film with no oscillations. The dimensionless group $\Delta g/g_0$ then compares the peak amplitude for changes in the apparent gravitational field against the background acceleration due to gravity. We will estimate these dimensionless groups for our reference observations at 10Hz and maximum volume (1cm peak-to-peak displacements), or approximately $20\text{m/s}^2 = 2g_0$. Under these conditions, fluid columns with approximate thickness 1mm were observed to climb up vertically-oriented surfaces.

To compute σ_0/σ^* , we will need estimates for both σ_0 and σ^* . With respect to the former, a steady falling film in fixed gravity gives a wall shear stress of $\sigma_0 = \rho g_0 h$, where h is the thickness of the fluid film in this case. From the experiments of Merkt et. al.

[14], we see evidence of discontinuous shear thickening from around shear stresses of 40Pa·s, and we use this as our estimate of σ^* . Assuming a fluid density of around 1.3g/cc and a film height of 1mm, this gives $\sigma_0/\sigma^* \approx 3$. Similarly, we estimate $\Delta g/g_0 \approx 2$.

It is worth noting that the ratio σ_0/σ^* is proportional to the film thickness, which our experiments did not directly control for. The selection of a preferred film thickness in experiments could reflect a “fastest rising” thickness but it might also simply be constrained by capillary effects: future work would be needed to explore this question.

In Figures 10(c) and (d), we see that model predictions show a net climbing behavior for $\sigma_0/\sigma^* \approx 3$ and $\Delta g/g_0 \approx 2$, though this does appear to lie very near to the boundary where climbing behaviors are predicted. In fact, the model suggests that thicker fluid films would also show climbing under these conditions - possibly even at a faster speed - but this was not observed. For this reason we note that the selection of a preferred film thickness for climbing may be more complex than what our naive modeling approach is prepared to consider.

Overall, we can confirm that at least one of our documented experimental observations lies quantitatively within the regime where climbing behaviors might be expected from our simple modeling approach. Qualitatively, our experiments also agree with Figure 10(c) and (d) in that a sufficiently large oscillating gravitational field is required to induce climbing behaviors, and that droplets/films will not climb if they are below a minimum thickness, i.e. low values of σ_0/σ^* . Beyond this, our experimental design was not sufficiently powerful or well-controlled to facilitate a more complete comparison with vibrated fluid film predictions of Figure 10.

5 Summary and Conclusions

The behavior of dense suspensions climbing up against oscillating gravity can be described in terms of an apparent “negative viscosity”, as average stress and shear rate are in opposite directions.

The Wyart-Cates model for dense suspensions is used to calculate shear rates and velocities. Average shear rates corresponding to oscillating stresses are first calculated. As with the stress hysteresis mechanism proposed in earlier work by Deegan, an apparent “negative viscosity” is only possible when the underlying flow curve exhibits discontinuous shear thickening (DST) or shear jamming (SJ): we find no such effect for fluids with continuous shear thickening (CST). With DST and SJ fluids, negative viscosity effects are more readily seen when (1) the particle fraction ϕ is close to random close packing ϕ_S , (2) oscillations in stress are slightly larger than the mean stress $\Delta\sigma/\sigma_0 > 1$,

and (3) averages stresses are comparable to the stress needed for frictional contacts to form. Square wave forcing appears to be most efficient at exploiting a fluid’s potential for climbing, since smoothly varying forcing protocols (e.g. sine-wave) are forced to spend more time exploring the non-inverted portion of the flow curve at positive shear rates, where large positive shear rates are sampled.

We believe that this apparent “negative viscosity” effect is likely relevant to a wide range of phenomena observed in VVDS. As a first line of inquiry, we provided calculations of the WC model for a falling film under vibrating gravity. There, it was indeed found that the discussion on oscillating shear flows was directly relevant to explaining the conditions under which the net velocity of the film was opposed to the average influence of gravity.

Finally, as a proof-of-principle measure, we conducted experiments on VVDS that show fluid droplets steadily climbing up a vertically oriented surface. These climbing droplets are a new phenomenon in VVDS and, in our opinion, more cleanly isolate the mechanism behind a broader range of climbing behaviors documented in the literature. When comparing some experimental observations against our modeling approach, we confirm that the observed climbing behavior are consistent with a parameter space where our WC modeling framework expects a “negative viscosity” effect to be observed. There are still open questions, however, including the selection of a preferred film thickness for climbing columns of fluid.

In future studies, and as constitutive modeling capabilities for dense suspensions improve, it will be interesting to repeat this analysis to account for (for example) the effects of fluid reversal and non-local rheology. More accurate experimental measurements can also be done to more completely characterize the phenomena of “climbing droplets” in VVDS. Future work may also explore a possible connection between climbing in VVDS and the classical mechanisms of normal stress differences and curved streamlines.

6 Acknowledgements

The authors would like to thank Romain Mari for sharing the results of Figure 4 with us, and for allowing us to include his work in our paper. We thank Prof Mike Cates for the support and helpful discussions that made this project possible. We are also grateful to an anonymous reviewer for their helpful suggestions and thoughtful discussion, especially in the introduction and section 4.2. Xingjian Hou thanks Dr Michal Kwasigroch and Dr Adam Boies for their guidance on research and funding. Work is funded by Trinity College Cambridge Projects Fund and by the European Research

Council under the Horizon 2020 Programme, ERC grant agreement number 740269.

References

- [1] JM Ottino and DV Khakhar. “Mixing and segregation of granular materials”. In: *Annual review of fluid mechanics* 32 (2000), pp. 55–91.
- [2] Cécile Clavaud et al. “Revealing the frictional transition in shear-thickening suspensions”. In: *Proceedings of the National Academy of Sciences* 114.20 (2017), pp. 5147–5152. DOI: 10.1073/pnas.1703926114. eprint: <https://www.pnas.org/doi/pdf/10.1073/pnas.1703926114>. URL: <https://www.pnas.org/doi/abs/10.1073/pnas.1703926114>.
- [3] B. M. Guy et al. “Constraint-Based Approach to Granular Dispersion Rheology”. In: *Phys. Rev. Lett.* 121 (12 Sept. 2018), p. 128001. DOI: 10.1103/PhysRevLett.121.128001. URL: <https://link.aps.org/doi/10.1103/PhysRevLett.121.128001>.
- [4] Abhinendra Singh, Jeffrey Morris, and Morton Denn. “Microstructural description of shear-thickening suspensions”. In: *EPJ Web of Conferences* 140 (Jan. 2017), p. 09023. DOI: 10.1051/epjconf/201714009023.
- [5] Neil Y. C. Lin et al. “Hydrodynamic and Contact Contributions to Continuous Shear Thickening in Colloidal Suspensions”. In: *Phys. Rev. Lett.* 115 (22 Nov. 2015), p. 228304. DOI: 10.1103/PhysRevLett.115.228304. URL: <https://link.aps.org/doi/10.1103/PhysRevLett.115.228304>.
- [6] Romain Mari et al. “Shear thickening, frictionless and frictional rheologies in non-Brownian suspensions”. In: *Journal of Rheology* 58.6 (2014), pp. 1693–1724.
- [7] Abhinendra Singh et al. “Shear Thickening and Jamming of Dense Suspensions: The “Roll” of Friction”. In: *Phys. Rev. Lett.* 124 (24 June 2020), p. 248005. DOI: 10.1103/PhysRevLett.124.248005. URL: <https://link.aps.org/doi/10.1103/PhysRevLett.124.248005>.
- [8] Matthieu Wyart and Michael E Cates. “Discontinuous shear thickening without inertia in dense non-Brownian suspensions”. In: *Physical review letters* 112.9 (2014), p. 098302.
- [9] M. E. Cates et al. “Jamming, Force Chains, and Fragile Matter”. In: *Phys. Rev. Lett.* 81 (9 Aug. 1998), pp. 1841–1844. DOI: 10.1103/PhysRevLett.81.1841. URL: <https://link.aps.org/doi/10.1103/PhysRevLett.81.1841>.
- [10] Ryohei Seto et al. *Shear jamming and fragility in dense suspensions*. Feb. 2019.

- [11] Christopher Ness, Romain Mari, and Michael E Cates. “Shaken and stirred: Random organization reduces viscosity and dissipation in granular suspensions”. In: *Science advances* 4.3 (2018), eaar3296.
- [12] Neil Y.C. Lin et al. “Tunable shear thickening in suspensions”. In: *Proceedings of the National Academy of Sciences* 113.39 (2016), pp. 10774–10778. ISSN: 0027-8424. DOI: 10.1073/pnas.1608348113. eprint: <https://www.pnas.org/content/113/39/10774>. URL: <https://www.pnas.org/content/113/39/10774>.
- [13] J. J. J. Gillissen et al. “Constitutive model for shear-thickening suspensions: Predictions for steady shear with superposed transverse oscillations”. In: *Journal of Rheology* 64.2 (2020), pp. 353–365. DOI: 10.1122/1.5129657. eprint: <https://doi.org/10.1122/1.5129657>. URL: <https://doi.org/10.1122/1.5129657>.
- [14] Florian S. Merkt et al. “Persistent Holes in a Fluid”. In: *Phys. Rev. Lett.* 92 (18 May 2004), p. 184501. DOI: 10.1103/PhysRevLett.92.184501. URL: <https://link.aps.org/doi/10.1103/PhysRevLett.92.184501>.
- [15] Stefan von Kann, Jacco H. Snoeijer, and Devaraj van der Meer. “Phase diagram of vertically vibrated dense suspensions”. In: *Physics of Fluids* 26.11 (2014), p. 113302. DOI: 10.1063/1.4900855. eprint: <https://doi.org/10.1063/1.4900855>. URL: <https://doi.org/10.1063/1.4900855>.
- [16] Troy Shinbrot et al. “Paradoxical ratcheting in cornstarch”. In: *Physics of Fluids* 27.10 (2015), p. 103101. DOI: 10.1063/1.4934709. eprint: <https://doi.org/10.1063/1.4934709>. URL: <https://doi.org/10.1063/1.4934709>.
- [17] Andrew Stephenson. “XX. On induced stability”. In: *The London, Edinburgh, and Dublin Philosophical Magazine and Journal of Science* 15.86 (1908), pp. 233–236. DOI: 10.1080/14786440809463763. eprint: <https://doi.org/10.1080/14786440809463763>. URL: <https://doi.org/10.1080/14786440809463763>.
- [18] Rahul Ramachandran and Michael Nosonovsky. “Vibro-levitation and inverted pendulum: parametric resonance in vibrating droplets and soft materials”. In: *Soft Matter* 10 (26 2014), pp. 4633–4639. DOI: 10.1039/C4SM00265B. URL: <http://dx.doi.org/10.1039/C4SM00265B>.
- [19] P. Brunet, J. Eggers, and R. D. Deegan. “Vibration-Induced Climbing of Drops”. In: *Phys. Rev. Lett.* 99 (14 Oct. 2007), p. 144501. DOI: 10.1103/PhysRevLett.99.144501. URL: <https://link.aps.org/doi/10.1103/PhysRevLett.99.144501>.
- [20] Stéphane Douady. “Experimental study of the Faraday instability”. In: *Journal of fluid mechanics* 221 (1990), pp. 383–409.

- [21] Robert D. Deegan. “Stress hysteresis as the cause of persistent holes in particulate suspensions”. In: *Phys. Rev. E* 81 (3 Mar. 2010), p. 036319. DOI: 10.1103/PhysRevE.81.036319. URL: <https://link.aps.org/doi/10.1103/PhysRevE.81.036319>.
- [22] Brad K Gibson. “Liquid mirror telescopes-history”. In: *Journal of the Royal Astronomical Society of Canada* 85 (1991), p. 158.
- [23] Isidro E. Zarraga, Davide A. Hill, and David T. Leighton. “Normal stresses and free surface deformation in concentrated suspensions of noncolloidal spheres in a viscoelastic fluid”. In: *Journal of Rheology* 45.5 (2001), pp. 1065–1084. DOI: 10.1122/1.1396356. eprint: <https://doi.org/10.1122/1.1396356>. URL: <https://doi.org/10.1122/1.1396356>.
- [24] Daniel Bonn et al. “Rod-Climbing Effect in Newtonian Fluids”. In: *Phys. Rev. Lett.* 93 (21 Nov. 2004), p. 214503. DOI: 10.1103/PhysRevLett.93.214503. URL: <https://link.aps.org/doi/10.1103/PhysRevLett.93.214503>.
- [25] Allen H Hoffman and William G Gottenberg. “Determination of the material functions for a simple fluid from a study of the climbing effect”. In: *Transactions of the Society of Rheology* 17.3 (1973), pp. 465–486.
- [26] Irvin M. Krieger and Thomas J. Dougherty. “A Mechanism for Non-Newtonian Flow in Suspensions of Rigid Spheres”. In: *Transactions of the Society of Rheology* 3.1 (1959), pp. 137–152. DOI: 10.1122/1.548848. eprint: <https://doi.org/10.1122/1.548848>. URL: <https://doi.org/10.1122/1.548848>.
- [27] Michael Cates. “Constitutive modeling of time-dependent flows in frictional suspensions”. In: *EPJ Web of Conferences* 249 (Jan. 2021), p. 01002. DOI: 10.1051/epjconf/202124901002.
- [28] Rahul N Chacko et al. “Dynamic vorticity banding in discontinuously shear thickening suspensions”. In: *Physical review letters* 121.10 (2018), p. 108003.
- [29] François Boyer, Olivier Pouliquen, and Élisabeth Guazzelli. “Dense suspensions in rotating-rod flows: normal stresses and particle migration”. In: *Journal of Fluid Mechanics* 686 (2011), pp. 5–25.
- [30] David L Henann and Ken Kamrin. “Continuum thermomechanics of the nonlocal granular rheology”. In: *International Journal of Plasticity* 60 (2014), pp. 145–162.
- [31] Peter D Olmsted. “Perspectives on shear banding in complex fluids”. In: *Rheologica Acta* 47.3 (2008), pp. 283–300.
- [32] Brice Saint-Michel, Thomas Gibaud, and Sébastien Manneville. “Uncovering instabilities in the spatiotemporal dynamics of a shear-thickening cornstarch suspension”. In: *Physical Review X* 8.3 (2018), p. 031006.

- [33] Vikram Rathee, Daniel L Blair, and Jeffrey S Urbach. “Localized stress fluctuations drive shear thickening in dense suspensions”. In: *Proceedings of the National Academy of Sciences* 114.33 (2017), pp. 8740–8745.
- [34] Baptiste Darbois Texier et al. “Surface-wave instability without inertia in shear-thickening suspensions”. In: *Communications Physics* 3.1 (2020), pp. 1–7.
- [35] *Online tone generator, author=Tomasz P. Szynalski, url=https://www.szynalski.com/tone-generator/, journal=Online Tone Generator - generate pure tones of any frequency, note = "[Online; accessed 10-Sep-2021]"*.
- [36] Romain Mari et al. “Nonmonotonic flow curves of shear thickening suspensions”. In: *Physical Review E* 91.5 (2015), p. 052302.